

SHAPING BIPOLAR AND ELLIPTICAL PLANETARY NEBULAE: EFFECTS OF STELLAR ROTATION, PHOTOIONIZATION HEATING, AND MAGNETIC FIELDS

GUILLERMO GARCÍA-SEGURA,¹ NORBERT LANGER,² MICHAŁ RÓŻYCZKA,^{3,4} AND JOSÉ FRANCO⁵

Received 1998 February 27; accepted 1999 January 4

ABSTRACT

We present two-dimensional hydrodynamical and magnetohydrodynamical simulations of the evolution of planetary nebulae formed through the interaction of two succeeding, time-independent stellar winds. Both winds are modeled according to a consistent physical prescription for the latitudinal dependence of their properties. We propose that single stars with initial masses above $\sim 1.3 M_{\odot}$ can achieve near-critical rotation rates during their “superwind” phase at the tip of the asymptotic giant branch (AGB). We show that the resulting equatorially confined winds and their subsequent inflation to a double lobe structure by the post-AGB wind leads to the typical hourglass shape found in many planetary nebulae, such as MyCn 18. Following Chevalier & Luo and Różyczka & Franco, we then combine the effect of a magnetic field in the post-AGB wind with rotating AGB winds. We obtain highly collimated bipolar nebula shapes, reminiscent of M2-9 or He 2-437. For sufficiently strong fields, ansae and jets, similar to those observed in IC 4593 are formed in the polar regions of the nebula. Weaker fields are found to be able to account for the shapes of classical elliptical nebulae, e.g., NGC 6905, in the case of spherically symmetric AGB winds, which we propose for single stars with initial masses below $\sim 1.3 M_{\odot}$. Photoionization, via instabilities in the ionization-shock front, can generate irregularities in the shape of the simulated nebulae. In particular, it leads to the formation of cometary knots, similar to those seen in the Helix nebula (NGC 7293). This effect may also be responsible for large-scale irregularities like those found in Sh 2-71 or WeSb 4. We arrive at a scenario in which the majority of the planetary nebula with their diverse morphologies is obtained from single stars. This scenario is consistent with the Galactic distribution of the different nebula types, since spherical and elliptical nebulae—which have a distribution with a large scale height above the Galactic plane—are ascribed to progenitor masses below $\sim 1.3 M_{\odot}$, with magnetic effects introducing ellipticities. Bipolar nebulae, on the other hand—which are on average closer to the Galactic plane—are found to stem from progenitors with initial masses above $\sim 1.3 M_{\odot}$.

Subject headings: ISM: magnetic fields — ISM: structure — MHD — planetary nebulae: general — stars: AGB and post-AGB — stars: mass loss

1. INTRODUCTION

Planetary nebulae (PNe) display a rich variety of shapes and have been cataloged in a series of morphological classes: bipolar, elliptical, point-symmetric, irregular, spherical, and quadrupolar (Chu, Jacoby, & Arendt 1987; Schwarz, Corradi, & Melnick 1992; Stanghellini, Corradi, & Schwarz 1993; Machado et al. 1996a, 1996b). In contrast, except for a few cases, dust shells around asymptotic giant branch (AGB) stars do not show signs of asphericity (Bujarrabal & Alcolea 1991; Kahane & Jura 1994; Stanek et al. 1995; Groenewegen 1996). Thus, during the transition from the AGB to the post-AGB phase, one or more physical processes responsible for the shape of these objects must be initiated. The origin of aspherical nebulae still remains as one of the fundamental problems of PNe formation and evolution (see reviews by Pottasch 1984; Iben 1993).

Recently, a detailed study of the differences between elliptical and bipolar nebulae has been done by Stanghellini et al. (1993) and Corradi & Schwarz (1995). They found that

the bipolar class has a scale height above the Galactic plane smaller than that for ellipticals (130 pc and 320 pc, respectively). Also, bipolars have the hottest central stars among PNe and display smaller deviations from pure circular Galactic rotation than other morphological types. In addition, bipolars also display the largest physical dimensions, have expansion velocities of up to 1 order of magnitude above the typical values of PNe, and show chemical overabundances of He, N, and Ne (see Torres-Peimbert & Peimbert 1997). These properties indicate that bipolar PNe are produced by more massive progenitors than are the remaining morphological classes. This conclusion, confirmed in an independent survey by Górny, Stasińska, & Tyłenda (1997), is in line with an earlier suggestion by Calvet & Peimbert (1983) that the bipolar nature of type I nebulae (Peimbert 1978) could be explained in terms of massive and quickly rotating progenitors (initial mass $M_i \geq 2.4 M_{\odot}$) that had to lose an appreciable fraction of their mass and angular momentum during the PN phase. If this is really the case, the main cause of bipolarity would be associated with the winds of rotating stars.

The structure and dynamics of winds from rotating stars have recently been described analytically by Bjorkman & Cassinelli (1993; hereafter BC93) and Ignace, Cassinelli, & Bjorkman (1996). For rotating stars, angular momentum conservation results in an equatorial “wind compression”: the outgoing particles of a rotating wind have orbits in a plane passing through the center of mass, such that the

¹ Instituto de Astronomía-UNAM, Apdo Postal 877, Ensenada, 22800 Baja California, Mexico; ggs@bufadora.astrosen.unam.mx.

² Institut für Physik, Universität Potsdam, D-14415 Potsdam, Germany; ntl@astro.physik.uni-postdam.de.

³ N. Copernicus Astronomical Center, Bartycka 18, 00-716 Warszawa, Poland; mnr@camk.edu.pl.

⁴ Member, Interdisciplinary Center for Mathematical and Computational Modeling, Banacha 2, 02-097 Warszawa, Poland.

⁵ Instituto de Astronomía-UNAM, Apdo Postal 70-264, 04510 México D. F., Mexico; pepe@astroscu.unam.mx.

wind density is increased at zones closer to the equatorial plane of the star and decreased toward the polar axis. The solutions of BC93 may provide a natural explanation for the origin of asphericity in winds from AGB stars (Ignace et al. 1996). According to this scheme, the density distributions resulting from rotating AGB winds are mainly governed by the ratio of the stellar rotational velocity to the critical rotational velocity, Ω .

The analytical results of BC93 have been confirmed with hydrodynamical simulations by Owocki, Cranmer, & Blondin (1994), but, given that the scheme assumes that the driving force is purely radial, they neglect some important nonradial force terms (such as those due to the oblate shape of the rotating star and gravity darkening) that modify the angular momentum of the outflowing particles and can reduce the amount of equatorial compression (Owocki, Cranmer, & Gayley 1996). These effects, which are certainly important for line-driven winds from hot stars, may be significantly less important for AGB winds (Langer 1997). Therefore, although a better description of wind acceleration requires the inclusion of nonradial components in the driving force, and the structure of the wind compressed region needs to be revised, the effect of equatorial compression as such is still likely to operate in rotating cool stars.

The idea that aspherical AGB winds can reproduce most PNe morphologies is not new, and it was already explored in previous hydrodynamical models (Icke 1988; Icke, Preston, & Balick 1989; Mellema, Eulderink, & Icke 1991; Icke, Balick, & Frank 1992; Frank & Mellema 1994; Dwarkadas, Chevalier, & Blondin 1996). It was argued that AGB wind asphericities could result from common envelope evolution, or, more generally, from the interaction of the AGB star with a binary companion (Livio 1993; Soker 1997, and references therein).

Asymmetries of the precursor AGB wind, however, are not the only factor responsible for the shaping of PNe. Gurzadyan (1969) discussed the possible role of magnetic fields in the structuring of PNe, and Pascoli (1992, and references therein) proposed that toroidal tubes can produce elongated and bipolar shapes. Similarly, using a steady state thin-shell solution for an axisymmetric MHD flow with a purely toroidal B field, Begelman & Li (1992) obtained elongated wind-driven bubbles generated by pulsar winds. The tension of the toroidal component in the magnetized wind (generated by stellar rotation) is responsible for the elongation. Following the same approach, Chevalier & Luo (1994) have also obtained aspherical steady state PNe structures from magnetized fast winds of rotating stars. More recently, with two-dimensional MHD simulations, Różyczka & Franco (1996) found that the time-dependent evolution of a magnetized shocked wind region has a very complex behavior, and collimated outflows with jetlike features can be created. The three-dimensional computations performed by García-Segura (1997) corroborates that the magnetized shocked gas indeed creates jets, and the only difference between the two-dimensional and three-dimensional results is that the collimated outflow in three-dimensional is, as expected, likely to be subject to kink instabilities. Thus, magnetic effects could be responsible for the generation of the collimated flows (jets) observed in some nebulae.

Here we extend the study of Różyczka & Franco (1996) and García-Segura (1997) to include the combined effects of rotation and magnetic fields in the interacting wind sce-

nario for the formation and evolution of PNe. Photoionization heating by the central star is also taken into account, and it is shown to be an important factor in generating PN shapes. For simplicity, we restrict the present survey to simple models in which the rotating winds, the ionizing fluxes, and magnetic fields originate from a single star and are constant in time. Readers interested in time-dependent winds or variable ionizing fluxes are referred to recent papers by Dwarkadas & Balick (1997), Mellema (1997), and García-Segura, Langer, & Mac Low (1996a), García-Segura et al. (1996b) in the context of massive stars.

The present paper is structured as follows: § 2 describes the relevant stellar parameters involved in the problem. Section 3 introduces the techniques used to perform the simulations. In § 4 we present hydrodynamical simulations with rotating AGB winds, including the effects of photoionization. Magnetohydrodynamical simulations, both for spherical and rotating AGB winds, are presented in § 5. Finally, § 6 presents a brief discussion, and § 7 summarizes our results.

2. RELEVANT STELLAR PARAMETERS

2.1. *The Rotation Rate of Thermally Pulsing AGB Stars*

Direct determinations of rotation rates for AGB stars are rare and mostly provide upper limits, of the order of a few kilometers per second. More rapid rotation, with $v \sin i \simeq 13 \text{ km s}^{-1}$, has been found in the case of V Hydrae, and it has been ascribed to the common envelope scenario (Barnbaum, Morris, & Kahane 1995). For single stars the rotation rate issue cannot be clarified because self-consistent evolutionary models of rotating stars from the main sequence into the AGB regime do not exist (see Chaboyer et al. 1995; Krishnamurthi et al. 1997). Hence, we derive in the following an evaluation of the stellar angular momentum at these evolved stages based on rough extrapolations of observational results at other evolutionary stages.

Given these restrictions, we discuss the single-star angular momentum evolution starting from the main sequence. According to observations, main-sequence stars in the initial mass range related to PN formation (from $\sim 0.8 M_{\odot}$ to about $5 M_{\odot}$) can be divided into two groups. Stars with masses below $\sim 1.3 M_{\odot}$ spin down during main-sequence evolution because of flares or magnetic winds that are tied up to their convective envelopes (Skumanich 1972; Carrasco, Franco, & Roth 1980; Soderblom, Duncan, & Johnson 1991). Recent helioseismology results indicate that these stars spin down as a whole, including their innermost parts (Tomczyk, Schou, & Thompson 1995; Kumar & Quartaert 1997), implying that they lose most of their initial angular momentum on the main sequence. When they expand to AGB dimensions, the resulting rotation velocities are below 0.01 km s^{-1} . Thus, these observations indicate that the expected rotation speeds of evolved low-mass stars (i.e., below $\sim 1.3 M_{\odot}$) should be very small.

Stars above $\sim 1.3 M_{\odot}$ do not have convective envelopes during core hydrogen burning, and they appear to remain as rapid rotators throughout their main sequence evolution (see, e.g., Sletteback 1970; Schrijver & Pols 1993). When they develop surface convection on their way to the red giant branch (RGB), they create a hydrogen-burning shell that separates the helium core from the envelope. It is then unclear if they are spun down by magnetic braking at these stages or conserve most of their angular momentum (Rutten

& Pylyser 1988; Schrijver & Pols 1993), and one may examine two alternative scenarios for the rotation of AGB stars: a slow-rotator, “pessimistic” case, and a fast-rotator, “optimistic” case. In the pessimistic case, post-main-sequence stars above $1.3 M_{\odot}$ would suffer magnetic braking and their helium cores are spun down by an efficient (yet unknown) coupling between the core and the envelope. Their further evolution would be similar to that of the lower mass stars. In the optimistic case, the helium core evolves decoupled from the envelope and retains its angular momentum; i.e., the entropy barrier of a nuclear burning shell prevents angular momentum from leaking out of the core. Also in this case, however, the angular momentum of the hydrogen envelope will be lost, either because of magnetic braking or mass loss and reexpansion of the convective envelope on the AGB (see Heger & Langer 1998).

When the stars move to the thermally pulsing AGB phase, the H- and He-burning shells periodically switch on and off. Thus the presumable barriers vanish periodically and core-envelope angular momentum exchange can occur during this stage. Such an exchange is very likely, since mixing of matter through the core boundary is known to occur in this phase, which is necessary to activate the $^{13}\text{C}(\alpha, n)$ neutron source and operate the *s*-process (Lambert et al. 1995). In the optimistic case, then, the helium core would remain as a fast rotator until angular momentum is redistributed during the thermal pulses. As the AGB stars may lose a large part of their envelope mass before the pulses and the PNe masses are of the order of $0.1 M_{\odot}$, one can assume that the core angular momentum is transferred, at the tip of the AGB, into an envelope of about $0.1 M_{\odot}$. To estimate the resulting rotational velocity of the envelope we may approximate the specific angular momentum of the core by its main sequence value. For a core of $\sim 0.5 M_{\odot}$ and a main-sequence radius of about $0.1 R_{\odot}$, we get $j \simeq 10^{17} \dots 10^{18} \text{ cm}^2 \text{ s}^{-1}$. Adopting an average radius of the envelope matter of $100 R_{\odot}$ on the AGB, we obtain a rotation velocity of

$$v_{\text{rot}} \simeq 10^{17.5} \text{ cm}^2 \text{ s}^{-1} \times 0.5 M_{\odot} / 100 R_{\odot} / 0.1 M_{\odot} \\ \simeq 2 \text{ km s}^{-1}. \quad (1)$$

Independent of this estimate, stars at the tip of the RGB or AGB may be subject of a significant spin-up of their surface layers, as recently pointed out by Heger & Langer (1998). They found that deep convective envelopes maintain most of their angular momentum while retreating in Lagrangian mass coordinate, and thus their specific angular momentum is drastically increased.

In this context it is also interesting to consider the recently obtained observational constraints on the rotation rates of white dwarfs. Heber, Napiwotzki, & Reid (1997) find upper limits in the range 18 to 43 km s^{-1} for $v \sin i$ for white dwarfs with masses above $\sim 0.65 M_{\odot}$ (roughly corresponding to initial masses above $1.3 M_{\odot}$), and between 8 and 18 km s^{-1} for less massive white dwarfs. For a typical white dwarf radius of $\sim 0.01 R_{\odot}$, the resulting maximum specific angular momentum is $j_{\text{max, WD}} \sim 10^{16} \text{ cm}^2 \text{ s}^{-1}$. This fact indicates that a substantial loss of angular momentum had to occur at some evolutionary stage, and it is conceivable that this stage was the transition period between the AGB phase and the white dwarf.

In summary, although it is possible that the hydrogen-rich envelope of low- and intermediate-mass stars could be

devoid of angular momentum at the beginning of the thermally pulsing AGB evolution, we propose that stars above $\sim 1.3 M_{\odot}$ can spin up their envelopes to rotational speeds of the order of 1 km s^{-1} , just prior to the PN ejection. Obviously, an even stronger spin-up effect could result from tidal interactions and common-envelope evolution if the AGB star were a component of a binary system (Soker 1997).

2.2. The Critical Rotation Rate at the Tip of the AGB

In order to evaluate whether a rotation rate of the order of 1 km s^{-1} can obtain the attribute “rapid,” we have to compare it with the rate of critical rotation. This is defined here as the rotation rate at which, in the equatorial plane, the centrifugal force balances the sum of all other forces at the surface of the star. However, in addition to the fact that an AGB star does not have a well-defined surface, the force balance in the external layers of its envelope is not yet well understood (Krüger, Gauger, & Sedlmayr 1994). This is particularly so for the phase during which the PN material is actually ejected from the star, since the responsible physical processes are not yet unambiguously identified. Recent work, based on the ideas of Lucy (1967) and Paczyński & Ziółkowski (1968), proposes a runaway expansion of the envelope, triggered by the luminosity and radius increase during a thermal pulse and maintained by the liberation of energy due to hydrogen recombination (Wagenhuber & Weiss 1994; Han, Podziadłowski, & Eggleton 1994). However, independently of physical details, we argue that in an envelope approaching such an instability the escape velocity, and thus the critical rotational velocity, approaches zero.

This situation is intriguingly similar to giant outbursts of so-called “luminous blue variables” (“LBVs”), which are thought to occur when these stars approach their Eddington luminosity $L_{\text{Edd}} = 4\pi cGM/\kappa$, with stellar mass M and opacity κ (Lamers & Fitzpatrick 1988). It has been shown by Langer (1997) that in this case the LBV, independently of its actual rotation rate, achieves critical rotation before it reaches the Eddington instability limit. In this situation, García-Segura, Langer, & Mac Low (1997) and Langer, García-Segura, & Mac Low (1999) found a slow, massive, equatorially confined outflow, which may later be inflated to a double-lobe structure by a fast spherically symmetric wind. The striking similarity of the shapes of some PNe and LBV nebulae—e.g., compare the “Hourglass Nebula” MyCn 18 with the “Homunculus Nebula” surrounding η Carinae—supports the idea that their common shape is due to a common underlying physical principle.

There are in fact two processes facilitating the formation of equatorially confined outflows from AGB stars, compared to LBVs. Ignace et al. (1996) have investigated rotating AGB winds and found that—because of their slow acceleration—considerable density contrasts can be obtained even for rotation at only 10% of the critical rotation rate. Furthermore, initial asymmetries in the AGB wind can be substantially amplified because of the strong dependence of the dust condensation rate on temperature, according to Dorfi & Höfner (1996).

Therefore, we propose here that values of $\Omega = v_{\text{rot}}/v_{\text{crit}}$ very close to 1 may be appropriate for AGB single stars above $\sim 1.3 M_{\odot}$ during the phase of PN ejection. We parametrize the “superwind” in the same way as the giant LBV outbursts in our previous works; i.e., we set the Eddington

parameter $\Gamma = L/L_{\text{Edd}}$ close to 1 and apply the Bjorkman & Cassinelli (1993) model for rotating stellar winds (see § 3). We emphasize that our approach, and the corresponding latitudinal dependence of the wind density, remains valid even in the case in which a force different from the radiation force is responsible for the superwind.

2.3. Magnetic Fields of AGB and Post-AGB Stars

The detection of strong magnetic fields ($B > 10^3$ G) in normal and degenerate stars is relatively easy, but direct measurements of moderate and weak fields ($B < 300$ G) are difficult to obtain (see reviews by Ledoux & Renson 1966; Garstang 1977; Chanmugam 1992). Thus, surface B fields similar to the one in the Sun (of only a few gauss), and their associated activity cycles, would be impossible to detect in distant stars.

Descendants of AGB stars, both isolated white dwarfs and white dwarfs in cataclysmic variables, display field strengths of up to 5×10^8 G and 7×10^7 G, respectively (Chanmugam 1992). Most white dwarfs, however, seem to have surface magnetic field values below $\sim 10^3$ G. Measurements of B for evolved giant and supergiant stars, on the other hand, are scarce (see Arge, Mullan, & Dolginov 1995). Reid et al. (1979) found strong circular polarization in the OH masers from U Ori and IRC +10420. The OH masers indicate fields of about 10 mG, located at regions of about 10^{15} cm from the photosphere, suggesting field strengths at the stellar surfaces in the range of 10–100 G. Field intensities at the surfaces of post-AGB stars have not been reported in the literature, except for white dwarfs.

For the lower main sequence, the detected B -field values of F, G, and K stars can reach values of up to 3×10^3 G (Marcy 1984), but M dwarfs can reach slightly higher values of 4×10^3 G (Johns-Krull & Valenti 1996). These fields are generally associated with magnetic spots covering a small fraction of the stellar surface. Most (if not all) of these main-sequence magnetic stars show regular field variations on timescales of the order of a few days to several weeks, and some low-mass stars show variations with longer timescales, of about 10 yr (Wilson 1978). The possible association between magnetic activity and rotation has been explored over the years and, among other relationships, there are correlations between the magnetic moment and angular momentum for both lower and upper main-sequence stars (Blackett 1947; Arge et al. 1995; Baluinas, Sokoloff, & Soon 1996). It is unclear if these correlations can be applied to rotating stars in general, but it seems logical to ascribe them to dynamo amplification in the presence of differential rotation (Kippenhahn 1973; Curtis & Ness 1986). Dynamo activity has much more support for long-term cycling in solar-type stars and for starspot phenomenology in evolved RS CVn stars, which are well correlated with rotation. The usual scaling is with the Rossby number and the magnetic diffusivity (see, e.g., Praderie et al. 1986). In the case of the upper main sequence, which is not relevant for our present discussion, peculiar A and B magnetic stars display fields in the range 3×10^2 to 6×10^3 (Borra & Landstreet 1980; Borra, Landstreet, & Thomson 1983; Bohlender et al. 1987; Johns-Krull & Valenti 1996). They are relatively common in stellar associations, indicating that they are relatively young (Garrison 1967; Borra et al. 1983), but these magnetic stars can also be found as field stars.

In the case of PNe progenitors, the cores of AGB stars

power the fast winds but there are no measurements of the fields at these cores. The data for main-sequence stars and white dwarfs described above, however, indicate that one can explore two interesting cases for the AGB cores; a strongly magnetic regime with surface fields of about 10^3 G, and a mildly magnetic regime with fields ranging from a few gauss to about 3×10^2 G. Also, it is tempting to use the magnetic moment–angular momentum correlations to set fixed prescriptions for the combination of rotation frequencies and surface field strengths. Given the complexity of the problem, and the lack of knowledge on the applicability range for the correlations, here we explore only the mildly magnetic regime and treat the rotation speeds and B fields as independent parameters.

2.4. The Ionizing Flux of Post-AGB Stars

Planetary nebulae are found to have central stars with masses in the range 0.5 – $1.2 M_{\odot}$ (Stanghellini et al. 1993). Post-AGB stars in this mass range have luminosities of $\log L/L_{\odot} \simeq 3$ – 4.5 and achieve maximum effective temperatures of $\log T_{\text{eff}} \simeq 4.8$ – 5.7 (Schönberner 1979, 1983; Böcker 1994). Based on these values and on the blackbody approximation, we estimate the maximum number of Ly α photons (F_{\star}) emitted from PN central stars to be in the range $F_{\star} \simeq 5 \times 10^{46}$ to $5 \times 10^{47} \text{ s}^{-1}$. As the post-AGB evolution starts at effective temperatures at which F_{\star} is basically zero, and we use constant Ly α fluxes averaged over 500–1400 yr (i.e., time covered by the hydrodynamic simulations presented below), values in the range $F_{\star} = 10^{45}$ – 10^{47} s^{-1} appear to be appropriate. Note that the assumed fluxes are consistent with assumed mass loss rates and velocities of the fast wind (models E–L have fast, low-density winds and large F_{\star} , while models M–V have slower and denser winds with smaller F_{\star}).

3. NUMERICAL TECHNIQUES

The simulations have been performed using the magneto-hydrodynamic code ZEUS-3D (version 3.4), developed by M. L. Norman and the Laboratory for Computational Astrophysics. This is a finite-difference, fully explicit, Eulerian code descended from the code described in Stone & Norman (1992). A method of characteristics is used to compute magnetic fields as described in Clarke (1996). ZEUS-3D does not include radiation transfer, but we have implemented a simple approximation to derive the location of the ionization front for arbitrary density distributions (see Bodenheimer, Tenorio-Tagle, & York 1979 and Franco, Tenorio-Tagle, & Bodenheimer 1989, 1990). This is done by assuming that ionization equilibrium holds at all times and that the gas is fully ionized inside the H II region. We perform the simulations in spherical polar coordinates (r, θ, Φ), with reflecting boundary conditions at the equator and the polar axis, and rotational symmetry assumed with respect to the latter. Thus, our models are effectively two dimensional, and the simulations are carried out in the meridional (r, θ) plane of the nebula. The position of the ionization front in any given direction (θ, ϕ) from the photoionizing source is given by $\int n^2(r, \theta, \phi)r^2 dr \approx F_{\star}/4\pi\alpha_B$. The models include the Raymond & Smith (1977) cooling curve above 10^4 K. For temperatures below 10^4 K, the unperturbed gas is treated adiabatically but the shocked gas region is allowed to cool down with the radiative cooling curves given by Dalgarno & McCray (1972) and MacDonald & Bailey (1981). Finally, the photoionized gas is always

kept at 10^4 K, so no cooling curve is applied to the H II regions (unless, of course, there is a shock inside the photoionized region).

Our grids consist of 200×180 equidistant zones in r and θ , respectively, with a radial extent of 0.1 pc and an angular extent of 90° . The innermost radial zone lies at $r = 2.5 \times 10^{-3}$ pc from the central star. These values are the same for all the simulations shown in Figures 1, 2, 3, and 4 (note that not all the models are shown at the same physical time). The equations for the stellar wind flow, which are utilized as inner boundary conditions in our calculations at the first five innermost radial zones, are similar to the equations given by Bjorkman & Cassinelli (1993) for the limit of large distance from the central star:

$$v_\infty(\theta) = \zeta v_{\text{esc}}(1 - \Omega \sin \theta)^\gamma \quad (2)$$

and

$$(4\pi r^2 \rho)_\infty(\theta) = \frac{\alpha}{2} \kappa \dot{M}_0 (1 - \Omega \sin \theta)^\xi / v_\infty(\theta), \quad (3)$$

where we set $\zeta = 1$, $\gamma = 0.35$, and $\xi = -0.43$ (see BC93). κ is a correction factor introduced to ensure that the total stellar mass-loss rate \dot{M}_0 obeys $\dot{M}_0 = \int 4\pi r^2 \rho(\theta) d\theta d\phi$ at the inner boundary of our grid (see Table 1). v_∞ is the terminal wind velocity, and $(4\pi r^2 \rho)_\infty$ is the terminal wind density times $4\pi r^2$, as a function of the polar angle θ . $\Omega = v_{\text{rot}}/v_{\text{crit}}$, and $v_{\text{crit}} = v_{\text{esc}}/\sqrt{2} = [GM(1 - \Gamma)/R]^{1/2}$, with M and R being mass and radius of the star, and Γ standing for the ratio L/L_{Edd} of stellar luminosity to Eddington luminosity. The quantity α is defined by

$$\alpha = \left[\cos \phi' + \cot^2 \theta \left(1 + \gamma \frac{\Omega \sin \theta}{1 - \Omega \sin \theta} \right) \phi' \sin \phi' \right]^{-1}, \quad (4)$$

with

$$\phi' = \frac{\Omega \sin \theta}{2\sqrt{2}} \frac{v_{\text{crit}}}{v_\infty(\theta)}, \quad (5)$$

and as such it differs from the corresponding BC93's quantity defined by their implicit formula (26). The strict use of

their equations would imply that, prior to density and velocity evaluation at a given location (r, θ) , their formulae (17) and (19) had to be iteratively solved to find θ_0 of the streamline passing through that location, while equations (2), (3), (4), and (5) can be solved explicitly. This difference came along originally through a misinterpretation of BC93's equations. However, since $\phi' < \pi/2$ in equation (5) for $\Omega \leq 0.995$, it has the advantage of avoiding the formation of wind compressed disks for large Ω , whose properties cannot be well predicted, and even their very existence is questionable (Owocki et al. 1994, 1996). At the same time, wind density and velocity distributions obtained from our approach agree quite well with those resulting from test computations based on original equations. To be more precise, our prescription gives almost the same results as that of BC93 provided a slightly different value of Ω is used. Both values of Ω are related by

$$\Omega_{\text{BC93}} = \Omega \Omega_{\text{th}}, \quad (6)$$

where Ω_{BC93} is the value to be inserted in BC93's equations, and Ω_{th} is the threshold value for the formation of a wind-compressed disk. As $\Gamma \rightarrow 1$ in our AGB scenario, Ω_{th} also approaches 1, so that $\Omega_{\text{BC93}} \sim \Omega$ (BC93; Ignace et al. 1996; J. E. Bjorkman 1997, private communication).

In our case the Eddington luminosity is given by radiation pressure on dust grains. The grains are formed in the expanding stellar atmosphere. As a realistic estimate of Γ for an AGB star is impossible because of the lack of knowledge of the optical properties of the recently formed grains, we assume a value of $\Gamma = 0.98$ for the AGB phase, which results in escape velocities comparable to the typical expansion velocities of PNe. The AGB star in all models is assumed to have a radius of $150 R_\odot$ and a mass of $2 M_\odot$, which, with $\Gamma = 0.98$, gives $v_{\text{esc}} = 10 \text{ km s}^{-1}$.

The values for the mass-loss rates and wind velocities in Table 1 are those commonly accepted for the formation of PNe in the interacting stellar wind model (Kwok, Purton, & Fitzgerald 1978; Kwok 1982, 1994; Kahn 1983; Balick 1987; Balick, Preston, & Icke 1987; Aller 1993). The values for the escape velocities v_{esc} given in Table 1 are those for the polar region ($\theta = 0$).

In §§ 4 and 5, we will employ winds obtained with values of $\Omega = 0, 0.5, 0.9$, and 0.98 . For $\Omega \leq 0.9$, the factor α in equation (3) plays only a minor role, as we find $\alpha \leq 1.32$ for

TABLE 1
WIND AND STELLAR PROPERTIES (INPUTS)

Model	Wind	\dot{M} ($M_\odot \text{ yr}^{-1}$)	v_{esc} (km s^{-1})	v_{crit} (km s^{-1})	v_{rot} (km s^{-1})	Ω	$\rho_{\text{eq}}/\rho_{\text{pl}}$	$v_{\text{pl}}/v_{\text{eq}}$
Models without Magnetized Fast Winds								
A, E, F	AGB	1×10^{-5}	10.	7.07	0.000	0.00	1.00	1.00
B, G, H	AGB	1×10^{-5}	10.	7.07	3.535	0.50	1.81	1.27
C, I, J	AGB	1×10^{-5}	10.	7.07	6.363	0.90	8.75	2.23
D, K, L	AGB	1×10^{-5}	10.	7.07	6.928	0.98	112.	3.92
A-L	Fast	1×10^{-7}	1000.	707.	100.	0.14	1.13	1.05
Models with Magnetized Fast Winds								
M, N	AGB	1×10^{-6}	10.	7.07	0.000	0.00	1.00	1.00
O, P	AGB	1×10^{-6}	10.	7.07	3.535	0.50	1.81	1.27
Q, R	AGB	1×10^{-6}	10.	7.07	6.363	0.90	8.75	2.23
S, T, U, V	AGB	1×10^{-6}	10.	7.07	6.928	0.98	112.	3.92
M-U	Fast	4×10^{-7}	500.	353.	100.	0.28	1.32	1.12
V	Fast	4×10^{-7}	200.	141.	100.	0.71	3.12	1.53

TABLE 2
NUMERICAL SAMPLE

Model	Ω_{AGB}	$\log F_{\star}$ (s^{-1})	σ
A	0.00	0	0
B	0.50	0	0
C	0.90	0	0
D	0.98	0	0
E	0.00	47	0
F	0.00	46	0
G	0.50	47	0
H	0.50	46	0
I	0.90	47	0
J	0.90	46	0
K	0.98	47	0
L	0.98	46	0
M	0.00	46	0.01
N	0.00	45	0.01
O	0.50	46	0.01
P	0.50	45	0.01
Q	0.90	46	0.01
R	0.90	45	0.01
S	0.98	46	0.01
T	0.98	45	0.01
U	0.98	45	0.1
V	0.98	45	0.1

all θ . The obtained equator-to-pole density contrasts are 1.81, 8.75, 112, with α being 1.03, 1.32, and 4.84, for $\Omega = 0.5, 0.9$, and 0.98 , respectively. The pole-to-equator velocity ratio is 1.28, 2.24, and 3.93, for the same three cases; i.e., the factor α that may be considered as the due to wind compression is never the dominant one. Even for $\alpha = 1$, a density contrast of more than 20 would have been obtained for $\Omega = 0.98$.

After the pioneering work of Weber & Davis (1967) to include the effects of rotation and magnetic fields in the solar wind, the solutions for steady magnetic winds from rotating stars have been developed for both the simple split-monopole (Sakurai 1985) and complex multipole configurations (see review by Rotstein 1998). The main feature of these steady state solutions is that the wind gets collimated toward the rotational axis by the toroidal magnetic field. This is the same basic mechanism that has been suggested to produce jets in magnetized accretion disks (see, e.g., Blandford & Payne 1982; Uchida & Shibata 1985; Sakurai 1987; Contopoulos 1995), and it is also the mechanism responsible for the elongation in the steady state solutions of interacting winds (Begelman & Li 1992; Chevalier & Luo 1994). The toroidal magnetic field component in the outflowing wind is (see, e.g., Parks 1991)

$$B_{\phi} = B_s \frac{v_{\text{rot}}}{v_{\infty}(\theta)} \left(\frac{R_s}{r} \right)^2 \left(\frac{r}{R_s} - 1 \right) \sin \theta, \quad (7)$$

where B_s and R_s are the magnetic field strength at the stellar surface and the stellar radius, respectively (note that B_s and R_s refer to the magnetized post-AGB star and should not be confused with the AGB). Equation (7) is a generalization of the standard formula for B_{ϕ} in the equatorial ($\theta = 90^\circ$) plane, which is adequate for the solar wind (J. R. Jokipii 1997, private communication). The function $\sin \theta$ cancels the toroidal component at the symmetry axis (note that in Różyczka & Franco 1996, θ is the astrometric latitude, and

$\theta = 0$ corresponds to the equator instead of the axis), but, as Różyczka & Franco (1996) have shown, the precise form of the off-equator distribution of the field is unimportant provided that the field is sufficiently strong to cause an appreciable deformation of the shocked wind region. The poloidal field component can be neglected, so that our field configuration naturally satisfies the condition $\nabla \cdot \mathbf{B} = 0$.

We assume that the field is frozen into the fast wind and is passively carried across the free fast wind region up to the stagnation shock at the inner boundary of the shocked fast wind region. In the following, for a given mass-loss rate our models will be identified by three parameters (see Tables 1 and 2). The first one is the ratio of the stellar rotational velocity to the critical velocity, Ω (note that even if the stellar angular momentum remains constant, Ω is not constant during the evolution of a star). The second parameter is the ratio of the magnetic field energy density to the kinetic energy density in the fast wind (Begelman & Li 1992):

$$\sigma = \frac{B^2}{4\pi\rho v_{\infty}^2} = \frac{B_s^2 R_s^2}{\dot{M}v_{\infty}} \left(\frac{v_{\text{rot}}}{v_{\infty}} \right)^2. \quad (8)$$

Finally, the third parameter is the value of the ionizing flux F_{\star} .

4. HYDRODYNAMICAL SIMULATIONS

We have first computed four simple cases (models A, B, C, and D) in which neither photoionization nor magnetic field have been included. These models allow us to study the differences in the resulting shapes caused only by different rotation rates at the AGB phase. The input mass-loss rates and velocities for each model are given in Table 1.

In Figure 1 models A, B, C, and D with $\Omega = 0.00, 0.50, 0.90, 0.98$, respectively, are shown at 1500 yr after the onset of the fast wind. Differences in density distributions of the AGB winds make the models to expand at different velocities. The polar ($\theta = 0$) expansion velocity is 38, 43, 52, and 63 km s^{-1} for models A, B, C, and D, respectively, while the equatorial velocities are 38, 29, 16, and 10 km s^{-1} .

As a result, we obtain the whole spectrum of shapes from spherical to extremely bipolar ones by varying just one parameter: the stellar rotation rate in the late AGB phase. It is worth noticing that the models develop dynamical instabilities, such as Vishniac (1983), Kelvin-Helmholtz, and Rayleigh-Taylor instabilities (see García-Segura & Mac Low 1995). However, their growth rates are most probably underestimated by our assumption of stationary fast winds (Dwarkadas & Balick 1997). This, and the low spatial resolution of the present calculations, do not allow for any quantitative analysis of their development.

4.1. Photoionization Effects

The effects of photoionization in numerical simulations of PNe have been recently explored by Mellema (1995, 1997) and Mellema & Frank (1995). They included a detailed treatment of the radiation transfer in the modeling of PNe. Here, however, we do not solve the radiative transfer problem and use only the simplified approach to H II region evolution described by García-Segura & Franco (1996). This approach, which provides the approximate location of the ionization front in expanding photoionized regions, assumes ionization equilibrium in all directions and is entirely sufficient for our purposes because we are not interested in following the evolution of the ionic species

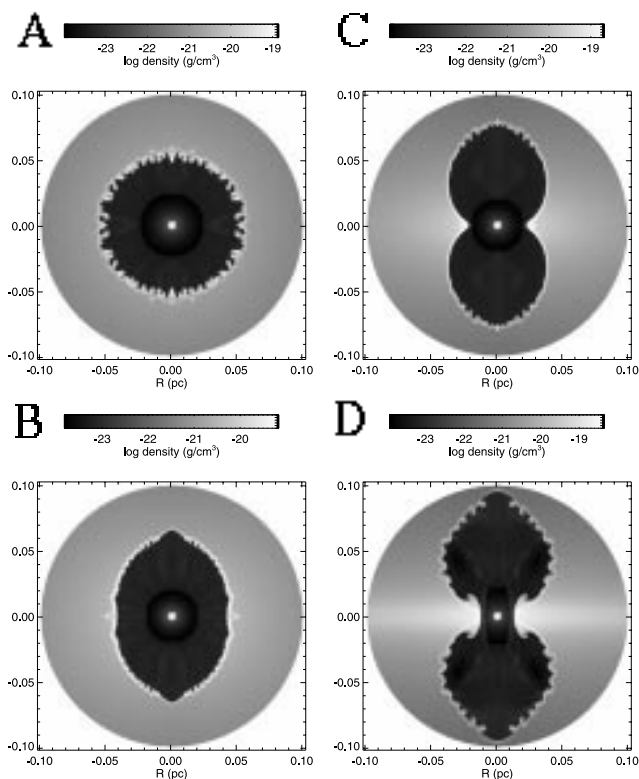


FIG. 1.—Models A ($\Omega_{\text{AGB}} = 0.00$, $\log F_{\star} = 0$), B ($\Omega_{\text{AGB}} = 0.50$, $\log F_{\star} = 0$), C ($\Omega_{\text{AGB}} = 0.90$, $\log F_{\star} = 0$), and D ($\Omega_{\text{AGB}} = 0.98$, $\log F_{\star} = 0$). Logarithm of density at $t = 1500$ yr after the onset of the fast wind. The instabilities are marginally resolved because of the poor resolution. The data has been reflected along the symmetry axis and the equator.

(comparisons with other codes that solve the radiative transfer problem give identical results to within 2% error; T. Freyer 1997, private communication).

We have obtained eight models (E–L, Fig. 2) that include the effects of the ionizing radiation (i.e., have nonzero F_{\star}). They are grouped in four pairs characterized by fixed Ω and σ , corresponding to Ω and σ of models A–D. Within each pair F_{\star} varies by a factor of 10, reflecting uncertainties of the value of the ionizing flux (see Tables 1 and 2). To facilitate the comparison with observations, we have also made snapshots of our model nebulae by plotting the emission measure of the photoionized region. To make a snapshot we rotated our two-dimensional model around the polar axis, reflected it with respect to the equator and projected it onto a plane inclined at 45° to the line of sight. Note that the snapshots give only a general outlook of the morphology of the nebula, and because of artificially imposed rotational symmetry they do not contain the whole information about its shape. Models E–L allow us now to visualize and estimate the effects of ionizing radiation on the dynamics of PNe.

The first important result is that the ionizing radiation can seriously alter the shape of PNe. With different F_{\star} , the same AGB and fast winds do not necessarily lead to the same shapes. In particular, a spherically symmetric AGB wind with small-scale density fluctuations can produce a nebula of irregular morphological type (compare models G and H in Fig. 2). Thus, ionization appears to be one of the main physical factors responsible for the origin of irregularities in the shells.

Second, the models clearly show that, at both large and small scales, the irregularities of the shape depend on how the ionizing radiation interacts with the dense shell between the fast wind and the AGB wind. In places where the ionization front is not trapped at all, the shells are much smoother and thicker because of the uniform thermal pressure. In regions where the ionization front is marginally trapped, vigorous dynamical instabilities develop because of the lack of uniformity. These ionization-driven instabilities operate in the same fashion as the elephant trunk instability discussed in Garcia-Segura & Franco (1996) (see § 6.2).

As in the previous section, we do not claim to have resolved the instabilities, and we stress that our results should be regarded as a qualitative description only. Note also that the bright heads of cometary knots resulting from ionization-driven instabilities are smeared into rings in our snapshots, such as those seen in model G (Fig. 2). Full three-dimensional simulations are needed to model them properly.

5. MAGNETOHYDRODYNAMICAL SIMULATIONS

Previous pilot studies were quite successful in recovering observational features concerning the shapes of PNe by including the stellar magnetic field. That fact strongly motivates the need of the MHD to study such a problem.

Following Reid et al. (1979), the appropriate magnetic parameters for the AGB wind should be in the range $\sigma \sim 10^{-4}$ to 10^{-5} . The magnetic effects are negligible for these σ values, and one could equally treat the AGB winds as non magnetic. The fast winds, however, should be explored with larger σ values (see below). Using the approach outlined at § 3, we have computed eight MHD models (M–T, Fig. 3) with magnetized fast winds. The models are grouped in pairs, characterized by fixed values of Ω and σ and varying F_{\star} by a factor of 10. Since MHD calculations consume more computational time than simple HD calculations, we have changed the values for the mass-loss rates and wind velocities in MHD models. In particular, the AGB mass-loss rate is now an order of magnitude smaller than in the previous HD models. This particular choice allows us to save computational time, since the expansion of the swept-up shell is faster (note that the physical times in figures 3 and 4 are shorter than those for figures 1 and 2) and does not affect the comparison with previous models from a morphological point of view. In all MHD models R_s is set equal to the solar radius, and B_s is assumed to be 254 G, resulting in $\sigma = 0.01$. This value is only slightly larger than solar ($\sigma_{\odot} = 0.009$; see Chevalier & Luo 1994).

We begin with nonrotating AGB winds, which in the absence of magnetic fields evolve into spherical nebulae. Our cases with $\Omega = 0$ (models M and N, Fig. 3) serve to visualize the changes that the magnetic field causes in the shapes of evolved nebulae. The general effect is the elongation of the nebula in the polar direction. The dense axial streams in our models are not resolved. However, the general tendency for stronger fields to produce more elongated nebulae is not affected by the resolution and/or axial effects. It is well known that two-dimensional calculations, in either cylindrical or spherical coordinates, could induce spurious effects on the rotation axis because the axis in these coordinate systems is a geometrical singularity; i.e., the gas is not allowed to pass through it. These reflective boundary effects are quite clear in models H and J (Fig. 2). The “jetlike” features appearing in our models are not

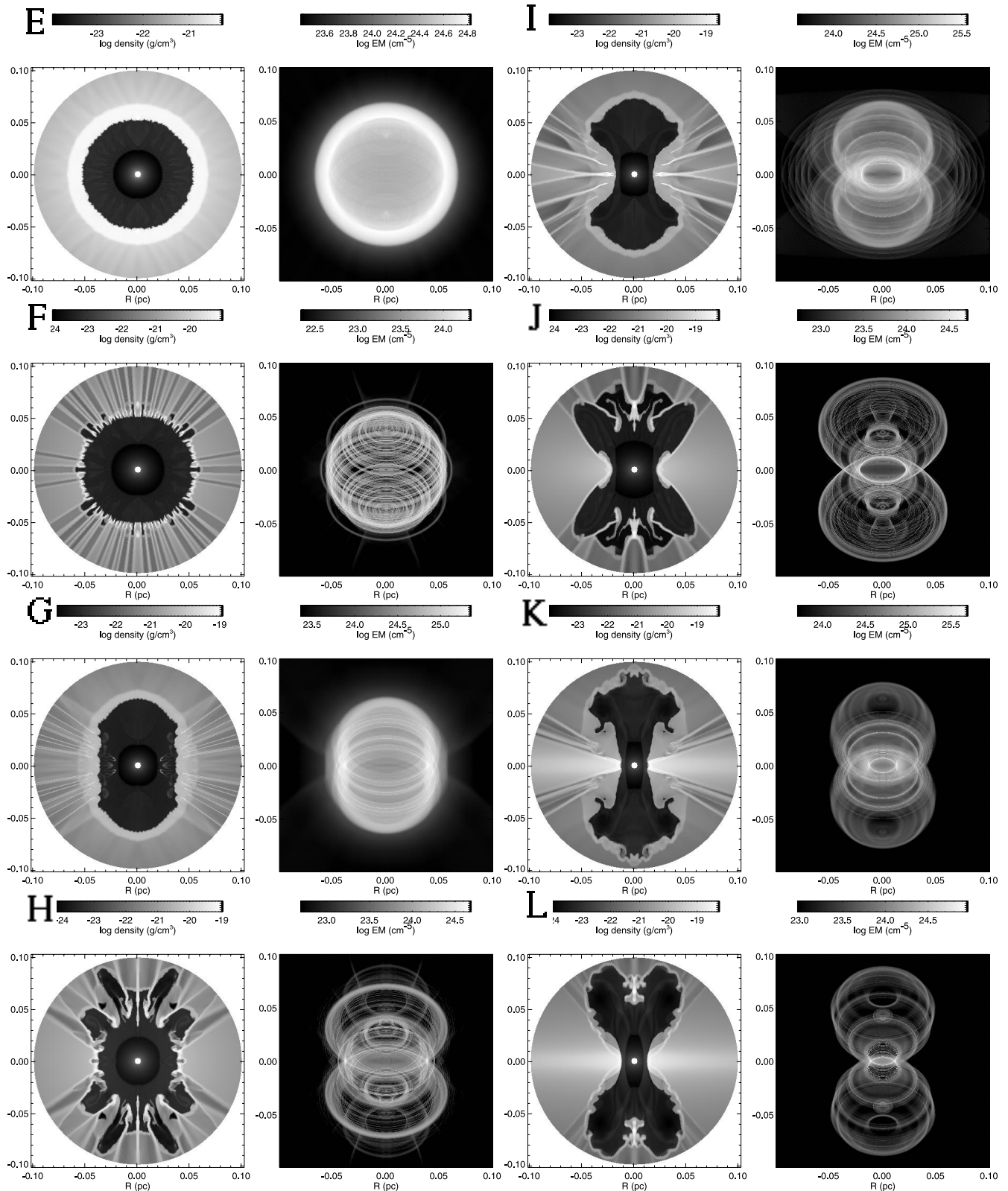


FIG. 2.—Models E ($\Omega_{\text{AGB}} = 0.00$, $\log F_{\star} = 47$), F ($\Omega_{\text{AGB}} = 0.00$, $\log F_{\star} = 46$), G ($\Omega_{\text{AGB}} = 0.50$, $\log F_{\star} = 47$), H ($\Omega_{\text{AGB}} = 0.50$, $\log F_{\star} = 46$), I ($\Omega_{\text{AGB}} = 0.90$, $\log F_{\star} = 47$), J ($\Omega_{\text{AGB}} = 0.90$, $\log F_{\star} = 46$), K ($\Omega_{\text{AGB}} = 0.98$, $\log F_{\star} = 47$), and L ($\Omega_{\text{AGB}} = 0.98$, $\log F_{\star} = 46$). Each model displays the logarithm of density at $t = 1500$ yr after the onset of the fast wind and the emission measure of the photoionized gas projected with a tilt of 45° from the plane of the sky.

totally associated with this issue (see Różyczka & Franco 1996; note also the clear tendency of the gas to pile up at the axis in model U in Fig. 4). The three-dimensional “axis-free” computations presented by García-Segura (1997)

show that the collimation is maintained even when kink instabilities are likely to appear. Thus, this formation mechanism for jets and ansae has been confirmed by three-dimensional calculations. A more detailed description of the

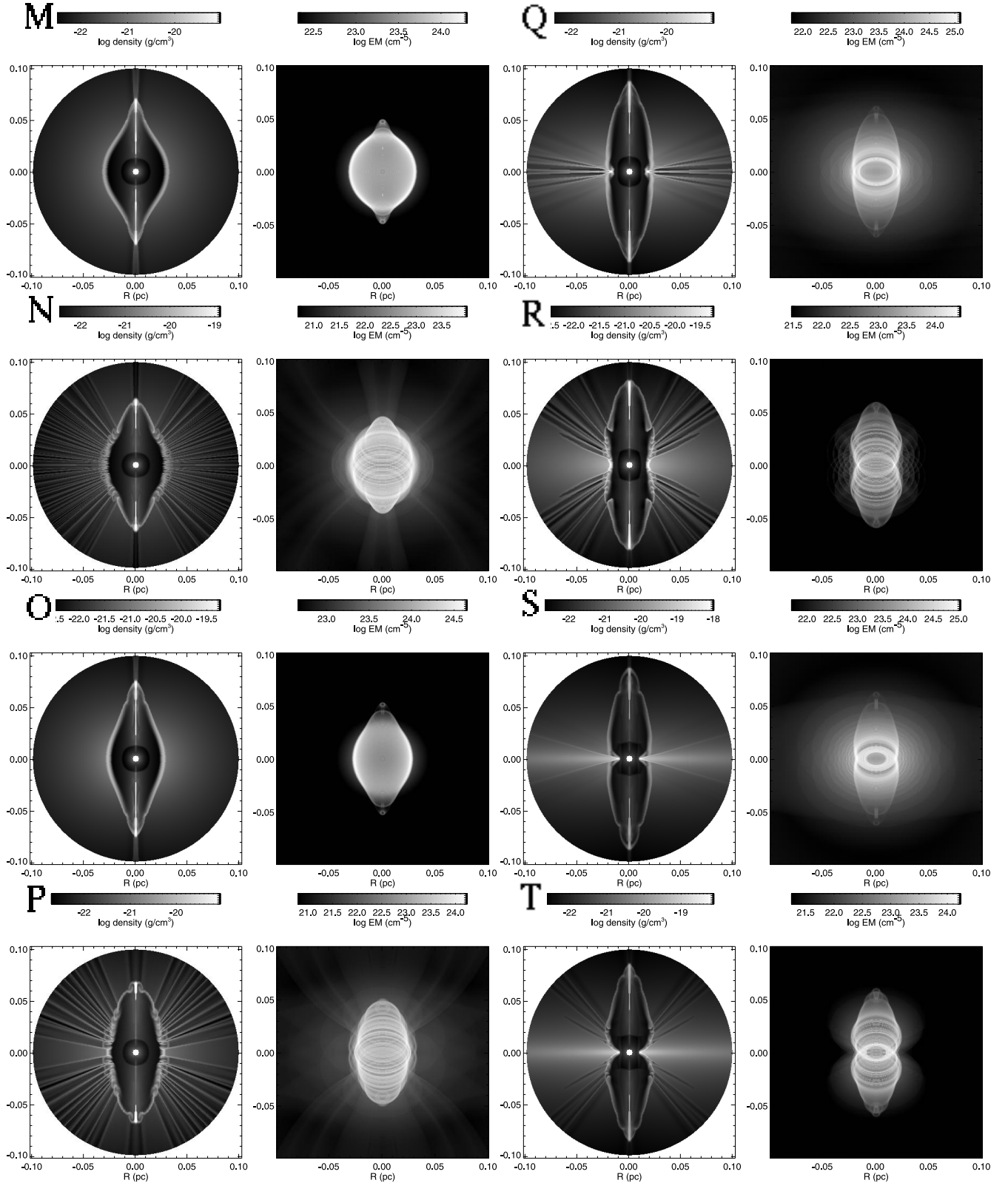


FIG. 3.—MHD models M ($\Omega_{\text{AGB}} = 0.00, \log F_{\star} = 46, \sigma = 0.01$), N ($\Omega_{\text{AGB}} = 0.00, \log F_{\star} = 45, \sigma = 0.01$), O ($\Omega_{\text{AGB}} = 0.50, \log F_{\star} = 46, \sigma = 0.01$), P ($\Omega_{\text{AGB}} = 0.50, \log F_{\star} = 45, \sigma = 0.01$), Q ($\Omega_{\text{AGB}} = 0.90, \log F_{\star} = 46, \sigma = 0.01$), R ($\Omega_{\text{AGB}} = 0.90, \log F_{\star} = 45, \sigma = 0.01$), S ($\Omega_{\text{AGB}} = 0.98, \log F_{\star} = 46, \sigma = 0.01$), and T ($\Omega_{\text{AGB}} = 0.98, \log F_{\star} = 45, \sigma = 0.01$). Each model displays the logarithm of density at $t = 400$ yr (M–R) and at $t = 367$ yr (S, T) after the onset of the fast wind and the emission measure of the photoionized gas projected with a tilt of 45° from the plane of the sky. Note the ansae formed at the pole from the magnetic tension.

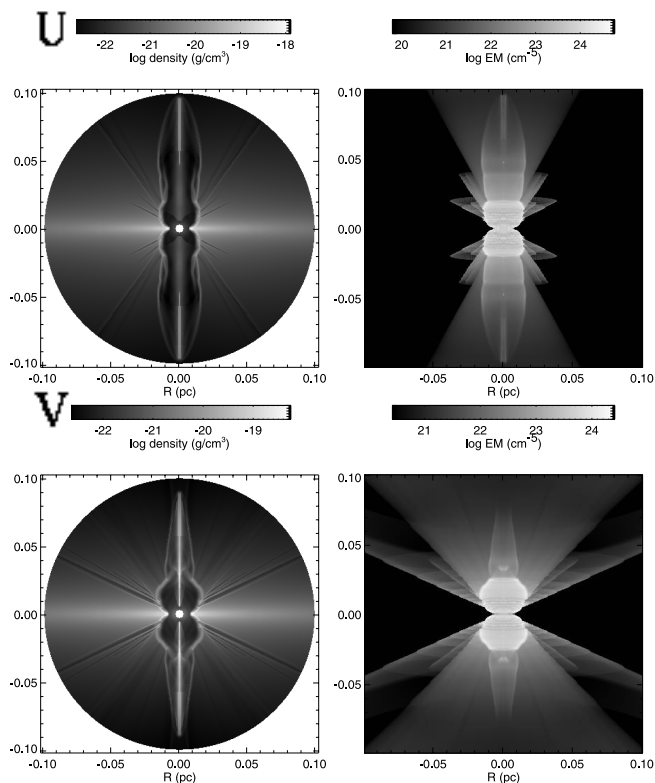


FIG. 4.—MHD Models U ($\Omega_{\text{AGB}} = 0.98$, $\log F_{\star} = 45$, $\sigma = 0.1$) and V ($\Omega_{\text{AGB}} = 0.98$, $\log F_{\star} = 45$, $\sigma = 0.1$). Same as Fig. 3, but $t = 200$ yr (U) and $t = 350$ yr (V). The projection is tilted 5° from the plane of the sky.

evolution of magnetized fast winds inside spherical AGB winds can be found in Chevalier & Luo (1994) and Różyczka & Franco (1996).

6. DISCUSSION OF RESULTS

The numerical catalog of PN shapes compiled in the present paper allows us to estimate the roles played in the shaping of PNe by three stellar properties: the rotation of the central star, the ionizing radiation, and the stellar magnetic field. We discuss these factors separately in the following sections.

6.1. Angular Momentum

The models presented in § 4 show that the assumption of rotation of the AGB star (close to its critical value) during its superwind phase, creates an equatorial compressed zone and results in bipolar nebular shapes. In fact, density contrasts $\rho_{\text{equator}}/\rho_{\text{pole}} > 2$, or, respectively, $\Omega > 0.5$, seem to be required in order to obtain a significant “waist” in the equatorial plane, i.e., a clearly bipolar morphology.

For $\Omega \geq 0.9$, we obtain a double-lobe structure, which is very reminiscent of the Homunculus nebula around the luminous blue variable star η Carinae (Humphreys & Davidson 1994). The shape of this nebula has been successfully reproduced by García-Segura et al. (1997) and Langer et al. (1999) using the same assumptions concerning the structure of the slow wind using $\Omega = 0.98$ as those described in § 3. Their conclusion is that a nearly critical rotation during the outburst of η Car, which ejected the material of the Homunculus, is the key property to obtain the double-lobe structure. Within the stellar mass range considered here, that outburst may be compared to the AGB superwind phase.

In fact, the basic morphological elements of the Homunculus nebula and several PNe (e.g., the “Hourglass Nebula” MyCn 18) are strikingly similar, suggesting that there is a common physical mechanism responsible for their formation. We propose that both LBVs and massive ($M_i > 1.3 M_{\odot}$) AGB stars can reach close-to-critical rotation during their giant outburst/superwind phase, as a consequence of a surface instability (e.g., the Eddington instability; see Langer 1997, 1998 for the LBV case).

According to this picture, and given that stars with initial masses below $\sim 1.3 M_{\odot}$ may lose most of their angular momentum during their main-sequence phase while more massive stars may retain a substantial fraction of it (see § 2.1), the bipolar PNe may result from more massive progenitors, while the amount of angular momentum left in stars with $M_i < 1.3 M_{\odot}$ might not be sufficient to break the symmetry in the mass outflow because of the superwind instability.

This line of thought is supported by the tighter concentration of bipolar PNe toward the Galactic plane as compared to PNe of other morphological types (Corradi & Schwarz 1995).

6.2. Radiation

Ionizing fronts behind thin shells can excite strong dynamical instabilities and lead to the formation of elephant trunks and other irregularities in H II regions. In particular, the I-S (ionization-shock) front instability operating in ionization fronts associated with radiative shocks (Giuliani 1979; García-Segura & Franco 1996) behaves very similar to the Vishniac instability (Vishniac 1983) and can produce finger-like structures. The effects of the Vishniac instability, reinforced by Rayleigh-Taylor instabilities, can be seen in the form of small-scale irregularities of the thin dense shell separating the fast wind from the AGB wind in Figure 1. The Vishniac instability is efficient in moving the shell gas transversely and decreasing the density in the so called “peaks” (i.e., the foremost regions of the perturbed shell; see García-Segura & Mac Low 1995) to the point at which the I-S front instability is excited. The peaks, which feel a faster propagation of the ionization front because of their lower density, are quickly heated by ionization. As a result, the perturbations grow faster and dense tails of neutral gas are formed, lagging behind the progressively rarefied peaks. Eventually, the ionizing photons escape from the peaks to ionize long streaks of the ambient medium in front of the shell (Fig. 2, model F; Fig. 3, model N). This is probably the case of the Dumbbell nebula (NGC 6853), which shows ionizing beams coming out of the nebula (Manchado et al. 1996a). On the other hand, the dense tails (or “cometary knots”) have large column densities and keep the ionization front trapped. They are characterized by a bright photoionized region at the head and a self-shielded neutral region in the form of a long tail pointing away from the central star (Fig. 2, model G). These structures might be related to the small-scale structures observed in the Helix nebula (NGC 7293) (Vorontsov-Velyaminov 1968; Meaburn et al. 1992).

Ionization-driven instabilities operate on a timescale comparable to the kinematic age of a planetary nebula (note that the sound speed of the ionized gas is comparable to the nebular expansion velocity of $\sim 10 \text{ km s}^{-1}$). Although it is not a general rule, the smaller the expansion velocity the more irregular will the nebula appear provided it is dense

enough to trap the ionizing photons. Models with $\Omega > 0$, in which the large-scale curvature of the shell varies along its surface because of the gradients of the AGB wind density, are particularly sensitive to changes in F_{\star} : a marginally trapped front leads here to significant modifications of the shape (compare models G and H or I and J in Fig. 2). Good observational examples of irregular nebulae most probably shaped by ionization-driven instabilities are Sh 2-71 and WeSb 4 (Manchado et al. 1996a), which show multiple knots, tails, and regions of high/low extinction.

On the other hand, when the nebula is not dense enough to trap the ionizing flux, the circumstellar gas gets fully ionized and its temperature (latter the thermal pressure) becomes homogeneous. The nebula then will become more and more spherical with time. This effect can be seen by comparing model A ($F_{\star} = 0 \text{ s}^{-1}$; Fig. 1) and model E ($F_{\star} = 10^{47} \text{ s}^{-1}$; Fig. 2): in the latter the corrugations of the shell caused by the Vishniac instability are almost entirely smoothed out. A similar result is found by Mellema (1997).

6.3. Stellar Magnetic Field

The toroidal field carried by the fast wind can constrain the motion of the flow, and an elliptical or bipolar nebula is produced even if the slow wind is spherically symmetric. The interaction of the two winds generates a hot wind-shocked region where the tension of the compressed B field generates an important new feature: a pair of flows are induced (one at each hemisphere) that move the gas toward the polar regions and create a pair of collimated outflows at the poles (Różyczka & Franco 1996). The basic features of the collimation mechanism are the following. First, the outer part of the magnetized shocked wind region becomes magnetically rather than thermally supported (i.e., the energy density of the compressed field grows larger than the thermal energy density). Then, the tension of the toroidal field slows down the expansion in the direction perpendicular to the symmetry axis (but the expansion in the direction parallel to the axis proceeds unimpeded), and, given that the intensity of the toroidal field decreases toward the axis, a magnetic pressure gradient in the z -direction exists. As a consequence and because of the hoop stress of the toroidal field, a flow in the shocked wind region toward the symmetry axis is initiated and maintained, leading to the formation of stagnation regions at the axis and to the formation of jets. Note that this mechanism works out similarly to that of magnetic confinement experiments in plasma laboratories (e.g., tokamaks, plasma guns). The gas that arrives at the polar regions of the nebula can form relatively dense blobs, depending of the radiative cooling conditions (García-Segura & López 1999), which may be identified with ansae observed in nebulae like NGC 6905.

Here we explore magnetic models with different values of Ω and present 10 models (see Table 1). As an initial case, and using a different coordinate system (spherical instead of cylindrical), we have confirmed that even in the case of $\Omega = 0$ it is possible to obtain elliptical nebulae for values of the field strength parameter σ close to the solar value of 0.009 (Chevalier & Luo 1994; Różyczka & Franco 1996); see models M and N in Figure 3.

In models O–T (Fig. 3) the AGB winds are aspherical because Ω is different from zero, and one can visualize the combined effects of rotation, magnetic fields and photoionization in the evolution of the nebulae. It was pointed out in § 4 that the most extreme bipolar shape obtained with the

formulation of Bjorkman & Cassinelli (1993) could be described by two tangential spheres (model D, Fig. 1). The corresponding magnetic model (model T, Fig. 3) has a well-defined spearhead shape. Again, the bulk effect of the magnetic field is the elongation of the nebulae in the polar direction. For $\sigma \sim 0.1$, a much higher degree of elongation (collimation) is achieved. Models U and V (Fig. 4) have surface magnetic field of 802 and 204 G, respectively, resulting in $\sigma = 0.1$. In these simulations, as before, bipolar nebulae are produced, but the magnetized shocked wind is so strongly collimated that it blows out of the nebula as a pair of jets. The ratio between the major and minor axes is 13.2 in model U. Such an elongation has never been obtained previously in the literature for a PN. Our models match pretty well the morphologies of M2-9 (Schwarz et al. 1997) and He 2-437 (Manchado et al. 1996a). The wind parameters are different in both cases (see tables 1 and 2), and the velocity of the fast wind in model V is much lower than in model U. As a result, a more strongly radiative terminal shock in Model V results in a narrower structure.

The above results are summarized in Figure 5, in which the PN shapes resulting for various combinations of Ω and σ are shown schematically. While the contribution from stellar rotation pushes the nebula upward on the diagram toward classical bipolars, the contribution from magnetic field shifts it horizontally toward more and more elongated (“squeezed”) objects.

It is now tempting to identify objects in which σ could be large enough for magnetic collimation to be operative. Unfortunately, there is no direct information available about stellar magnetic fields during the transition between the AGB phase and white dwarfs. Recent observations of nonthermal radio emission in A 30 (Dgani, Evans, & White 1998; Dgani & Soker 1998) indicate very low σ values for the wind of that nebula. This is expected in the framework of our model since the shape of A 30 is spherical. Some general trends, however, can be deduced based on the differences between elliptical and bipolar nebulae discussed by Stanghellini et al. (1993) and Corradi & Schwarz (1995). They found that within the bipolar class, which roughly corresponds to type I of Peimbert (Peimbert 1978), progeni-

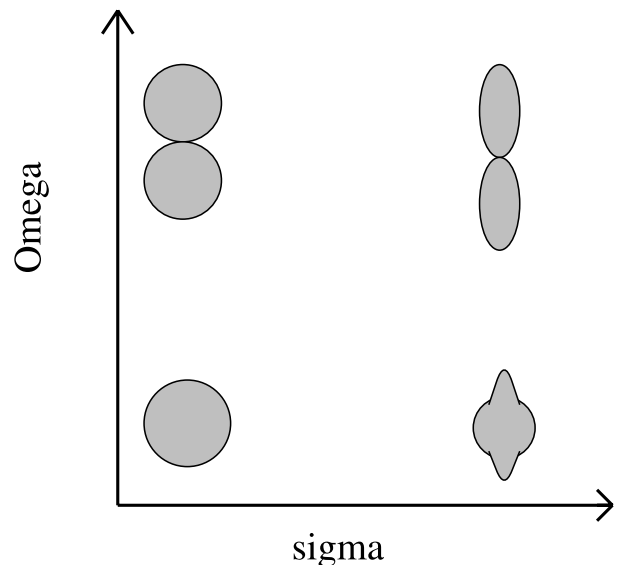


FIG. 5.—Schematic distribution of the PN morphology in the contribution of rotation (Ω) and magnetic field (σ).

tors of the nebulae are more massive than within other morphological classes. Also, bipolar PNe have significantly larger expansion velocities than spherical or elliptical ones. These two facts taken together seem to indicate that central stars of bipolar nebulae have more powerful winds. Because $\sigma \propto 1/(Mv_\infty^3)$, more powerful winds translate into lower σ (unless B_s correlates with the mass of the star). If it is really so, there should be an anticorrelation between the mass of the progenitor and the degree of magnetic collimation, in the sense that on the average the latter should be less efficient for more massive stars. Lower efficiency of magnetic collimation means increased percentage of regular "classical" bipolars generated by purely hydrodynamical effects. Thus, we arrive at a physical scenario that is qualitatively consistent with the observations, i.e., elliptical nebulae (low progenitor masses) are magnetically shaped, while classical bipolar nebulae (large progenitor masses) are shaped by rotation.

This however does not exclude that magnetic effects could be present in bipolars. As an example, echelle observations of the hourglass nebula (MyCn 18) by Bryce et al. (1997) show the appearance of high-velocity outflows coming out from the lobes in a point-symmetric mode. This example and others usually named as BRETS (bipolar, rotating jets; López, Steffen, & Meaburn 1997; López et al. 1998; see review by López 1997) tell us that magnetic effects can also play a role in bipolars, forming a pair of jets at the polar regions, even though rotation is the main physical mechanism determining their main shapes, i.e., a well defined equatorial waist.

Magnetic collimation is also the most successful mechanism up to now in explaining the point-symmetric nebulae (for the case of stellar winds, see García-Segura 1997; for the case of accretion disk winds, see Livio & Pringle 1997; Livio 1997).

Finally, we suggest that magnetic effects may also play a significant role in protoplanetary nebulae, in which partially ionized winds with relatively low velocities of $\sim 10^2$ km s $^{-1}$ are observed (Arrieta 1999). Again, because σ scales like v_∞^{-3} , high degrees of collimation, which could account for the origin of "FLIERs" and jets at the initial evolutionary stages of PNe (Balick 1993), are conceivable.

6.4. Verifying the Models

A comparison of the morphologies in observed nebulae with those resulting from the computed models provides a first test of the model goodness.

A second verification can be performed with the kinematics of nebulae and, specifically, with the fast outflows/jets that have been reported for several PNe during this last decade. Examples with fast outflows (~ 500 km s $^{-1}$ or higher) are He 2-437 (Riera et al. 1995) and MyCn 18 (Bryce et al. 1997). The observed large velocity values are hardly explained by invoking only hydrodynamical effects (Frank, Balick, & Livio 1996), since they are above the critical velocity of ~ 150 km s $^{-1}$ for which interstellar shocks become adiabatic. Magneto-hydrodynamical effects, on the other hand, are very efficient in forming these fast collimated outflows, as discussed in § 6.3.

In order to verify whether the MHD models can reproduce the range of observed velocities, Figure 6 shows the expansion velocity of the jet that appears in model U (Fig. 4) as it would be observed with a synthetic slit covering only the jet positions (1–2 on the figure). The model has been tilted 45° for a qualitative comparison with MyCn 18. The left panel of Figure 6 agrees quite well with Figure 3a in Bryce et al. (1997), although the model was not specifically intended to reproduce this nebula. The most remarkable feature is the approximately linear increase of the expansion velocity along the jet, which matches the actual echelle

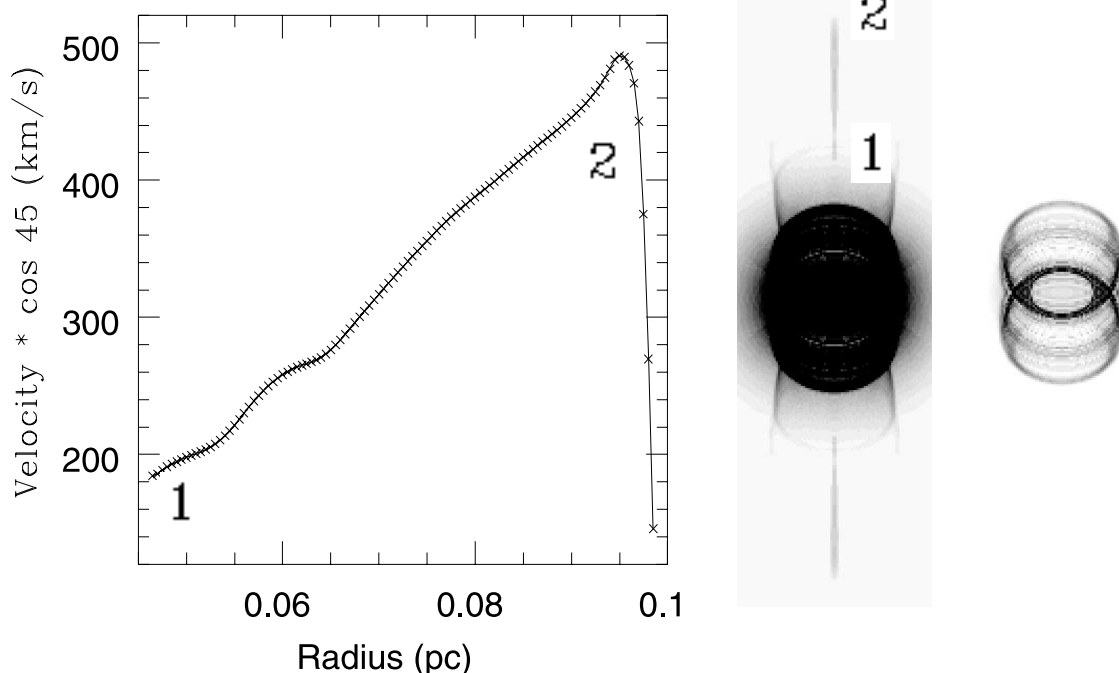


FIG. 6.—Projected expansion velocity of the model U jet tilted 45° from the plane of the sky is shown on the left. Crosses represent grid point values, and the solid line the interpolation. The labels "1" and "2" delimit an artificial slit along the jet shown in the middle panel. The middle and right panels are linear gray-scale representations of the emission measure of model U.

observations. This accelerative behavior is produced by the relaxation of the magnetic pressure in the shocked region. For completeness, the middle and right panels in Figure 6 display two synthetic images of the emission measure of the gas, which can be also compared with Figure 1 in Bryce et al. (1997). The qualitative agreement is striking.

Most observed jets in PNe, including the cases of He 2-437, MyCn 18, and Flemming 1, are composed by a stream of blobs. The current interpretation is that they are due to episodic ejections (see review by López 1997). Although this is certainly a possibility, one can also invoke MHD instabilities in a magnetized outflow. Magnetically confined plasmas by toroidal fields can develop kink, sausage, or neck instabilities (see, e.g., Jackson 1962), which can easily lead to the formation of blobs along the collimated plasma flow. For instance, the neck instability can be stabilized or saturated when the trapped poloidal component on the field is large enough ($B_z^2 > \frac{1}{2}B_\phi^2$). Note that the poloidal component in our computations is negligible, and the toroidal component, for example in the jet of model U (which is the strongest magnetized model), is 10^{-3} G. Then, the instability can occur but the resolution in our simulations cannot resolve its appearance and evolution. Another possibility is the MHD Kelvin-Helmholtz instability (Chandrasekhar 1961, p. 481), which, given the conditions of the collimated flow, is very likely to appear as well, probably combined with kink and neck instabilities.

A third issue is the formation of wind-compressed zones. This is difficult to verify in stars at the tip of the AGB phase because the winds are optically thick. Millimeter array observations could probably be used as a direct test for this idea.

A closely related issue is the existence of photoionization and photodissociation fronts in PNe. The ionization fronts are clearly visible in nearby PNe (because of the high angular resolution), as in NGC 7293, where the ionization fronts are located in each of the resolved blobs (Meaburn et al. 1992). New images of NGC 3132 by the *Hubble Space Telescope* also appear to show blobs in the nebula. The angular resolution is probably here the key problem. Obviously, the blobs can be formed by instabilities and the fronts delineate the locations at which the blobs become optically thick. The presence of molecular gas at the equatorial regions of most bipolar PNe (see the review by Torres-Peimbert & Peimbert 1997) also suggests that the ionization front is trapped somewhere inside the expanding envelope and further indicates the existence of a photodissociation region (PDR) separating the molecular phase from the ionized one (Natta & Hollenbach 1998 and references therein). Note that in our models for bipolars, the equatorial density enhancements remain always neutral until the end of the runs. Photodissociation fronts might have the same sort of dynamical effects as ionization fronts at the initial stages, but their importance decreases with time because the pressure gradients at the molecular/neutral interphases are small compared to those at the neutral/ionized boundaries (Diaz-Miller, Franco, & Shore 1998).

It is worthwhile to quote a paragraph from Balick (1987), since his interpretation is in line with our results: “*Local ionization conditions can, and often do, seemingly depart from the nebular average. Sudden drops in the ionization state that surround the outer edge of a nebula (NGC 2438, 6720, 7048, 7139, IC 418, 972, Abell 82, He 1-4) are normally interpreted*

to be the result of ionization fronts where the nebula becomes opaque to the ionizing radiation from the central star. A number of nebulae show such ionization fronts only in very selected portions of their boundary (NGC 650-1, 2346, 2440, 6445, 6543, 6781, 7026, IC 5217). Such nebulae all have relatively complex morphologies. One does not expect that they are optically thick to the stellar ionizing photons in all directions.”

The last issue concerns the low ionization state observed in the formed jets, blobs, and ansae (FLIERs). At the moment we cannot provide a quantitative result to compare with observations, since the computations do not include a detailed treatment of the different ionization species. However, the small-scale structures that appear in our simulations are dense and optically thick to the radiation field from the central star. Thus, their ionization state should be probably influenced by collisions.

7. SUMMARY AND CONCLUSIONS

In the present paper, we have studied the formation and evolution of planetary nebulae in the framework of the interacting stellar winds scenario (Kwok 1982; Balik 1987, 1988), by means of two-dimensional (“two-and-a-half”) MHD models. The parameters for the two successive stellar winds were based on the considerations of the angular momentum evolution of single stars of different initial masses, and assuming moderate values of the magnetic field in the surface of the progenitor star. The results of our models allow us to draw the following conclusions.

1. Because of the possibility that single stars with initial masses above $1.3 M_\odot$ retain rapidly spinning cores until they reach the tip of the AGB (§ 2.1) and the transport of angular momentum from the core into the envelope during the thermal pulses, such stars may be close to critical rotation during their superwind phase (see § 2.2) with the consequence of the formation of strongly bipolar PNe (see Fig. 1).
 2. As a common physical origin for the shapes of bipolar planetary nebulae and nebulae around luminous blue variables—which is suggested by the striking similarity of some of them—we propose close-to-critical rotation during the phase of strong mass loss (i.e., giant outburst or superwind phase, respectively), as a consequence of the occurrence of a surface instability (e.g., the Eddington instability).
 3. Single stars with initial masses below $\sim 1.3 M_\odot$ can not retain enough angular momentum (§ 2.1) to produce bipolar PNe (see models A, E, F, M, and N in Figs. 1, 2, and 3).
 4. A magnetic field in the post-AGB wind—as motivated by Chevalier & Luo (1994) and Różyczka & Franco (1996)—has a pronounced effect on the resulting nebula shape and leads to typical elliptical shapes (see Fig. 3).
 5. Strong fields in post-AGB winds combined with significant rotation lead to highly collimated bipolar nebulae and jets (see Fig. 4).
 6. In optically thick swept-up shells, ionization fronts can introduce numerous instabilities that affect the nebula shape significantly and that cannot be suppressed by magnetic fields. With different F_\star , the same AGB and fast winds do not necessarily lead to the same shapes. PNe classified as irregular type can be reproduced by such instabilities.
- In summary, our models cover the majority—though not all—of the observed PN morphologies by relying on a

single-star scenario for the nebula shaping. However, close binary evolution is expected to affect the morphology of a fraction of PNe (see, e.g., Soker 1998). Some channels of close binary evolution may lead to physical situations similar to those considered in the present paper. For example, the merging of an AGB star with a companion star or a planet (Soker 1996) may lead to a spin-up of the AGB envelope and consequently to bipolar nebulae. However, although other explanations may exist, our scenario of single-star effects dominating the morphology of PNe is supported by the tighter concentration of bipolar PNe toward the Galactic plane as compared to elliptical PNe (Corradi & Schwarz 1995) and, independently, by their chemical composition (Peimbert 1978; Calvet & Peimbert 1983).

We thank our anonymous referee for his comments, which improved the paper considerably. We specially thank A. Arrieta, U. Heber, J. A. López, M.-M. Mac Low, A. Manchado, M. Peimbert, S. N. Shore, and S. Torres-Peimbert for fruitful discussions and comments. We thank

J. Bjorkman for useful comments and for providing us with his code and G. Mellema for the use of his tools in the visualizations. We thank Michael L. Norman and the Laboratory for Computational Astrophysics for the permission to use ZEUS-3D. Part of this work was done during the INAOE Guillermo Haro Workshop 1997 "Stellar/Gas Interactions," and we are thankful to all participants for very stimulating discussions. The computations were performed at Instituto de Astrofísica de Canarias, the Supercomputer Center of the Universidad Nacional Autónoma de México, Rechenzentrum Garching of the Max-Planck-Gesellschaft, and the Instituto Nacional de Astrofísica, Óptica y Electrónica. This work was partially supported by DGAPA-UNAM grant IN130698, CONACyT grant 400354-5-4843E, by the Deutsche Forschungsgemeinschaft through grants La 587/15-1 and La 587/16-1, and by a R&D CRAY Research grant. M. R. acknowledges partial support from the Committee for Scientific Research through the grants 2P 304 017 07 and 2P.03D.004.13.

REFERENCES

- Aller, L. H. 1993, in IAU Symp. 155, Planetary Nebulae, ed. R. Weinberger & A. Acker (Dordrecht: Kluwer), 1
- Arge, C. N., Mullan, D. J., & Dolginov, A. Z. 1995, ApJ, 443, 795
- Arrieta, A. 1999, in preparation
- Balick, B. 1987, AJ, 94, 671
- . 1988, AJ, 97, 476
- . 1993, in IAU Symp. 155, Planetary Nebulae, ed. R. Weinberger & A. Acker (Dordrecht: Kluwer), 131
- Balick, B., Preston, H. L., & Icke, V. 1987, AJ, 94, 1641
- Baluinas, S., Sokoloff, D., & Soon, W. 1996, ApJ, 457, L99
- Barnbaum, C., Morris, M., & Kahane, C. 1995, ApJ, 450, 862
- Begelman, M., & Li, Z. Y. 1992, ApJ, 397, 187
- Bjorkman, J. E., & Cassinelli, J. P. 1993, ApJ, 409, 429 (BC93)
- Blackett, P. M. S. 1947, Nature, 159, 658
- Blandford, R. D., & Payne, D. G. 1982, MNRAS, 199, 883
- Blöcker, T. 1994, A&A, 299, 755
- Bodenheimer, P., Tenorio-Tagle, G., & Yorke, H. W. 1979, ApJ, 233, 85
- Bohlender, D. A., Brown, D. N., Landstreet, J. D., & Thomson, I. B. 1987, ApJ, 323, 325
- Borra, E., & Landstreet, J. D. 1980, ApJS, 42, 421
- Borra, E., Landstreet, J. D., & Thomson, I. B. 1983, ApJS, 53, 151
- Bryce, M., López, J. A., Holloway, A. J., & Meaburn, J. 1997, ApJ, 487, L161
- Bujarrabal, V., & Alcolea J. 1991, A&A, 251, 536
- Calvet, N., & Peimbert, M. 1983, Rev. Mexicana Astron. Astrofis., 5, 319
- Carrasco, L., Franco, J., & Roth, M. 1980, A&A, 86, 217
- Chaboyer et al. 1995, ApJ, 441, 876
- Chandrasekar, S. 1961, Hydrodynamic and Hydromagnetic Stability (London: Clarendon Press)
- Chanmugam, G. 1992, ARA&A, 30, 143
- Chevalier, R. A., & Luo, D. 1994, ApJ, 421, 225
- Chu, Y.-H., Jacoby, G. H., & Arendt, R. 1987, ApJS, 64, 529
- Clarke, D. A. 1996, ApJ, 457, 291
- Contopoulos, J. 1995, ApJ, 450, 616
- Corradi, R. L. M., & Schwarz, H. E. 1995, A&A, 293, 871
- Curtis, S. A., & Ness, N. F. 1986, J. Geophys. Res., 91, 11003
- Dalgarno, A., & McCray, R. A. 1972, ARA&A, 10, 375
- Dgani, R., Evans, N. J., & White, S. M. 1998, preprint
- Dgani, R., & Soker, N. 1998, ApJ, 499, L83
- Diaz-Miller, R. L., Franco, J., & Shore, S. N. 1998, ApJ, 501, 192
- Dorfi, E. A., & Höfner, S. 1996, A&A, 313, 605
- Dwarkadas, V. V., & Balick, B. 1997, BAAS, 191, 15.05
- Dwarkadas, V. V., Chevalier, R. A., & Blondin, J. M. 1996, ApJ, 457, 773
- Franco, J., Tenorio-Tagle, G., & Bodenheimer, P. 1989, Rev. Mexicana Astron. Astrofis., 18, 65
- . 1990, ApJ, 349, 126
- Frank, A., Balick, B., & Livio, M. 1996, ApJ, 471, L53
- Frank, A., & Mellema, G. 1994, A&A, 289, 937
- García-Segura, G. 1997, ApJ, 489, L189
- García-Segura, G., & Franco, J. 1996, ApJ, 469, 171
- García-Segura, G., Langer, N., & Mac Low, M.-M. 1996a, A&A, 316, 133
- . 1997, in ASP Conf. Ser. 120, Luminous Blue Variables: Massive Stars in Transition, ed. A. Nota & H. J. G. L. M. Lamers (San Francisco: ASP), 332
- García-Segura, G., & López, J. A. 1999, in preparation
- García-Segura, G., & Mac Low, M.-M. 1995, ApJ, 455, 160
- García-Segura, G., Mac Low, M.-M., & Langer, N. 1996b, A&A, 305, 229
- Garrison, R. 1967, ApJ, 147, 1003
- Garstang, R. H. 1977, Rep. Prog. Phys., 40, 105
- Giuliani, J. L. 1979, ApJ, 233, 280
- Górny, K. S., Stasińska, G., & Tylenda, R. 1997, A&A, 318, 256
- Groenewegen, M. A. T. 1996, A&A, 305, L61
- Gurzadyan, G. A. 1969, The Physics and Dynamics of Planetary Nebulae (Springer: Berlin)
- Han, Z., Podsiadlowski, P., & Eggleton, P. P. 1994, MNRAS, 270, 121
- Heber, U., Napiwotzki, R., & Reid, I. N. 1997, A&A, 323, 817
- Heger, A., & Langer, N. 1998, A&A, 334, 210
- Humphreys, R. M., & Davidson, K. 1994, PASP, 106, 1025
- Iben, I., Jr. 1993, in IAU Symp. 155, Planetary Nebulae, ed. R. Weinberger & A. Acker (Dordrecht: Kluwer), 587
- Icke, V. 1988, A&A, 202, 177
- Icke, V., Balick, B., & Frank, A. 1992, A&A, 253, 224
- Icke, V., Preston, H. L., & Balick, B. 1989, AJ, 97, 462
- Ignace, R., Cassinelli, J. P., & Bjorkman, J. E. 1996, ApJ, 459, 671
- Jackson, J. D. 1962, Electrodynamics (New York: Wiley), 482
- Johns-Krull, C. M., & Valenti, J. A. 1996, ApJ, 459, L95
- Kahane, C., & Jura M. 1994, A&A, 290, 183
- Kahn, F. D. 1983, in IAU Symp. 103, Planetary Nebulae, ed. D. R. Flower (Dordrecht: Kluwer), 305
- Kippenhahn, R. 1973, Stellar Chromospheres, ed. S. Jordan & E. H. Avrett, NASA SP-317 (Washington, DC: NASA), 275
- Krishnamurthi, A., et al. 1997, ApJ, 480, 303
- Krüger, D., Gauger A., & Sedlmayr, E. 1994, A&A, 290, 573
- Kumar, P., & Quataert, E. J. 1997, ApJ, 475, L143
- Kwok, S. 1982, ApJ, 258, 280
- . 1994, PASP, 106, 344
- Kwok, S., Purton, C. R., & Fitzgerald, P. M. 1978, ApJ, 219, L125
- Lambert, D. L., Smith, V. V., Busso, M., Gallino, R., & Straniero, O. 1995, ApJ, 450, 302
- Lamers, H. J. G. L. M., & Fitzpatrick E. 1988, ApJ, 324, 279
- Langer, N. 1997, in ASP Conf. Ser. 120, Luminous Blue Variables: Massive Stars in Transition, ed. A. Nota & H. J. G. L. M. Lamers (San Francisco: ASP), 83
- . 1998, A&A, 329, 551
- Langer, N., García-Segura, G., & Mac Low, M.-M. 1999, ApJ, submitted
- Ledoux, P., & Renson, P. 1966, ARA&A, 4, 326
- Livio, M. 1993, in IAU Symp. 155, Planetary Nebulae, ed. R. Weinberger & A. Acker (Dordrecht: Kluwer), 279
- . 1997, in IAU Symp. 180, Planetary Nebulae, ed. H. J. Habing & H. J. G. L. M. Lamers (Dordrecht: Kluwer), 74
- Livio, M., & Pringle, J. E. 1997, ApJ, 486, 835
- López, J. A. 1997, in IAU Symp. 180, Planetary Nebulae, ed. H. J. Habing & H. J. G. L. M. Lamers (Dordrecht: Kluwer), 197
- López, J. A., Meaburn, J., Bryce, M., & Holloway, A. J. 1998, ApJ, 493, 803
- López, J. A., Steffen, W., & Meaburn, J. 1997, ApJ, 485, L697
- Lucy, L. B. 1967, AJ, 72, 813
- MacDonald, J., & Bailey, M. E. 1981, MNRAS, 197, 995
- Manchado, A., Guerrero, M., Stanghellini, L., & Serra-Ricart, M. 1996a, The IAC Morphological Catalog of Northern Galactic Planetary Nebulae (Tenerife: Instituto de Astrofísica de Canarias)
- Manchado, A., Stanghellini, L., & Guerrero, M. 1996b, ApJ, 466, L95
- Marcy, G. W. 1984, ApJ, 276, 286

- Meaburn, J., Walsh, J. R., Clegg, R. E. S., Walton, N. A., Taylor, D., & Berry, D. S. 1992, *MNRAS*, 255, 177
- Mellema, G. 1995, *MNRAS*, 277, 173
- . 1997, *A&A*, 321, L29
- Mellema, G., Eulderink, F., & Icke, V. 1991, *A&A*, 252, 718
- Mellema, G., & Frank, A. 1995, *MNRAS*, 273, 401
- Natta, A., & Hollenbach, D. 1998, *A&A*, 337, 517
- Owocki, S. P., Cranmer, S. R., & Blondin, J. M. 1994, *ApJ*, 424, 887
- Owocki, S. P., Cranmer, S. R., & Gayley, K. G. 1996, *ApJ*, 472, L115
- Paczyński, B., & Ziółkowski, J. 1968, *Acta Astron.*, 18, 255
- Parks, G. K. 1991, *Physics of Space Plasmas: An Introduction* (New York: Addison-Wesley)
- Pascoli, G. 1992, *PASP*, 104, 350
- Peimbert, M. 1978, in *IAU Symp. No 76, Planetary Nebulae: Observations and Theory*, ed. Y. Terzian (Dordrecht: Reidel), 215
- Pottasch, S. R. 1984, *Planetary Nebulae. A Study of Late Stages of Stellar Evolution* (Dordrecht: Reidel)
- Praderie, F., Catala, C., Simon, T., & Boesgaard, A. M. 1986, *ApJ*, 303, 311
- Raymond, J. C., & Smith, B. W. 1977, *ApJS*, 35, 419
- Reid, M. J., Moran, J. M., Leach, R. W., Ball, J. A., Johnston, K. J., Spencer, J. H., & Swenson, G. W. 1979, *ApJ*, 227, L89
- Riera, A., García-Lario, P., Machado, A., Pottasch, S. R., & Raga, A. C. 1995, *A&A*, 302, 137
- Rotstein, N. O. 1998, *Fundam. Cosmic Phys.*, 19, 91
- Różyczka, M., & Franco, J. 1996, *ApJ*, 469, L127
- Rutten, R. G. M., & Pylyser, E. 1988, *A&A*, 191, 227
- Sakurai, T. 1985, *A&A*, 152, 121
- . 1987, *PASJ*, 39, 821
- Schönberner, D. 1979, *A&A*, 79, 108
- . 1983, *ApJ*, 272, 708
- Schrijver, C. J., & Pols, O. R. 1993, *A&A*, 278, 51
- Schwarz, H. E., Aspin, C., Corradi, R. L. M., & Reipurth, B. 1997, *A&A*, 319, 267
- Schwarz, H. E., Corradi, R. L. M., & Melnick, J. 1992, *A&AS*, 96, 23
- Skumanich, A. 1972, *ApJ*, 171, 565
- Sletteback, A. 1970, in *Stellar Rotation*, ed. A. Sletteback (Dordrecht: Reidel), 3
- Soderblom, D. R., Duncan, D. K., & Johnson, D. R. H. 1991, *ApJ*, 375, 722
- Soker, N. 1996, *ApJ*, 460, L53
- . 1997, *ApJS*, 112, 487
- . 1998, *ApJ*, 496, 833
- Stanek, K. Z., Knapp, G. R., Young, K., & Phillips, T. G. 1995, *ApJS*, 100, 169
- Stanghellini, L., Corradi, R. L. M., & Schwarz, H. E. 1993, *A&A*, 276, 463
- Stone, J. M., & Norman, M. L. 1992, *ApJS*, 80, 753
- Tomczyk, S., Schou J., & Thompson, M. J. 1995, *ApJ*, 448, L57
- Torres-Peimbert, S., & Peimbert, M. 1997, in *IAU Symp. 180, Planetary Nebulae*, ed. H. J. Habing & H. J. G. L. M. Lamers (Dordrecht: Kluwer), 175
- Uchida, Y., & Shibata, K. 1985, *PASJ*, 37, 515
- Vishniac, E. T. 1983, *ApJ*, 274, 152
- Vorontsov-Velyaminov, B. A. 1968, in *IAU Symp. 34, Planetary Nebulae*, ed. D. E. Osterbrock & C. R. O'Dell (Dordrecht: Reidel), 256
- Wagenhuber, J., & Weiss A. 1994, *A&A*, 290, 807
- Weber, E. J., & Davis, L. 1967, *ApJ*, 148, 217
- Wilson, O. C. 1978, *ApJ*, 226, 379